

Correlated topological phases in 3D complex oxides via Green's functions

Ara Go,¹ William Witczak-Krempa,² Gun Sang Jeon,³ Kwon Park,⁴ and Yong Baek Kim^{2,4}

¹*Department of Physics and Astronomy and Center for Theoretical Physics,
Seoul National University, Seoul 151-747, Korea*

²*Department of Physics, University of Toronto, Toronto, Ontario M5S 1A7, Canada*

³*Department of Physics, Ewha Womans University, Seoul 120-750, Korea*

⁴*School of Physics, Korea Institute for Advanced Study, Seoul 130-722, Korea*

(Dated: February 22, 2012)

We examine the effects of correlations on 3D topological insulators (TIs) as well as topological Weyl semimetals by using cellular dynamical mean-field theory (CDMFT). A model relevant to the pyrochlore iridates, a family of complex oxides that might harbour such phases, is used. We characterize the evolution of the topologically protected surface states and their disappearance for sufficiently strong interactions. We verify the bulk-boundary correspondence for correlated TIs by computing the quantized magneto-electric response coefficient using the interacting Green's function. This invariant also identifies a correlated axion insulator between a TI and Weyl semimetal, a feature absent in a simple mean-field treatment. We describe consequences for experiments and for the search for correlated materials with symmetry-protected topological order.

INTRODUCTION

The interplay of symmetry and topology has recently proven a rich avenue for the discovery of new phases of matter, some of which have been experimentally identified. A striking example is prediction and subsequent observation of two- and three-dimensional topological (band) insulators [1, 2]. The symmetry-protected topological orders in such phases cannot be fully characterized by conventional order parameters. They can, however, display universal electromagnetic response and/or robust boundary states. These effects are a manifestation of the fact that their ground state wavefunction contains non-trivial quantum entanglement [3].

In this work, we explore the quantum many-body effects in 3D symmetry-protected topological phases using cellular dynamical mean-field theory (CDMFT) [4, 5]. In contrast to the examples studied earlier in the context of non-interacting or single-particle picture, the Green's functions of interacting electrons obtained in CDMFT are used to characterize the effects of interactions on the bulk topological properties and boundary states. In particular, this makes it possible to explicitly compute topological invariants of interacting electrons in a microscopic model. We explore the correlation effects on 3D topological insulators (TIs) protected by time-reversal symmetry (TRS) or inversion symmetry, as well as on a closely related gapless phase dubbed a topological semimetal with Weyl-like quasiparticles [6–9]. These effects are examined in the context of a strongly correlated electronic Hamiltonian which is microscopically motivated from the studies of pyrochlore iridates [6, 10–13].

TRS-protected topological *band* insulators can be precisely characterized by a topological invariant in terms of the single-particle wavefunction. Such an approach cannot be applied in the presence of interactions, in which case one cannot use the sharp single-particle description put forth by band theory. Rather, one can ask if there exists a universal and quantized physical response of the system to a given external perturbation. For quantum Hall states the response function is the quantized Hall conductivity, while for TIs, it is the magneto-electric effect [14]: an externally applied electric field on the sample generates a parallel magnetic field, and vice versa. Such a response is quantized, the response coefficient depending solely on universal constants. It was argued on the grounds of topological field theory that the magneto-electric effect remains a well-defined topological response in the presence of interactions [14]. Moreover, a topological index was given in terms of the full interacting electronic Green's function. As some of the considerations in the establishment of such an invariant are rather abstract, it would be desirable to have a concrete verification of such an important claim. Here, we shall provide an explicit evaluation of this topological index in a model of interacting complex oxides.

A complimentary aspect of the quantized magneto-electric effect is the presence of protected surface states. We corroborate this bulk-boundary correspondence by analysing our interacting model in a finite-slab geometry. We do find that the TI surface states are robust to interactions, thus establishing the bulk-boundary connection for an interacting system and providing a check for the non-trivial topological index.

The model which we shall use as a platform to explore these phases has the added advantage of being relevant to a wide class of 3D complex oxides, the pyrochlore iridates. These materials, and closely related Iridium-based ones, are currently under close experimental scrutiny due to recent proposals for topological phases [6, 10–13]. As correlations seem to be an important factor in these *d*-electron compounds, our work could be instrumental in their

analysis. This being said, we emphasize that as we are dealing with topological phases, many of our results are expected to hold in general. Indeed, we envision that our methods can be fruitfully used in the analysis of correlated symmetry-protected topological ordered states and combined with *ab initio* tools in the quest for experimentally relevant candidate materials [15].

MODEL

We consider the following Hubbard Hamiltonian for the Iridium d -electrons hopping on a pyrochlore lattice with onsite Coulomb repulsion [13]:

$$H = \sum_{\langle \mathbf{R}i, \mathbf{R}'i' \rangle, \sigma\sigma'} ([T_o]_{\sigma\sigma'}^{ii'} + [T_d]_{\sigma\sigma'}^{ii'}) c_{\mathbf{R}i\sigma}^\dagger c_{\mathbf{R}'i'\sigma'} - \mu \sum_{\mathbf{R}i, \sigma} c_{\mathbf{R}i\sigma}^\dagger c_{\mathbf{R}i\sigma} + U \sum_{\mathbf{R}i} n_{\mathbf{R}i\uparrow} n_{\mathbf{R}i\downarrow}, \quad (1)$$

where $c_{\mathbf{R}i\sigma}$ annihilates an electron with the pseudospin σ at the i th basis site of the Bravais lattice vector \mathbf{R} . The index i runs from 1 to 4 and labels the corners of a tetrahedron. The hopping matrix T_o arises from oxygen-mediated hopping between the Ir atoms [10] with amplitude t , while T_d from the Ir-Ir hopping due to the *direct* overlap between the d -orbitals. The latter depends on two energy scales, t_σ and t_π , arising from the σ - and π -bonding between the d -orbitals, respectively. The chemical potential, μ , is such that each Ir atom contributes a single pseudospin-1/2 electron. The pseudospin arises from the combined effect of crystal fields and spin-orbit coupling [16]. Finally, the Hubbard repulsion U generates correlations by penalizing double occupation and thus drives the system away from simple single-particle physics. (We shall use the oxygen hopping strength, t , as our comparison scale.)

The phase diagram of the above Hamiltonian was previously analyzed by treating the onsite repulsion within a mean-field Hartree-Fock (HF) approach [13], which allows for a single-particle description. It was found that for small U/t , one obtains strong topological insulator and metallic phases, depending on the ratios of t_σ/t and t_π/t . At sufficiently large U , the system becomes magnetic. Near the transition, i.e. for small enough magnetization, it was found that the topological Weyl semimetal (TWS) arises. Here, we shall focus on two representative sets of hopping parameters, $t_\sigma/t = 1$ or -1 , with the ratio $t_\pi/t_\sigma = -2/3$ fixed. The first one, being at the center of our analysis, is such that the HF mean-field theory predicts that the system undergoes transitions from a TI to a TWS, and to a magnetic antiferromagnet as one increases U . The second set of hoppings corresponds to the transition from a semimetal to a magnetic Mott insulator, passing through a “tilted Weyl semimetal”.

We use the above model to examine the fate of these phases and transitions within CDMFT. CDMFT has been widely used to investigate correlated microscopic models [5] but only recently was it applied to topological phases [17], specializing to two dimensions. As we will deal with robust topological properties, most of our results will hold generically. We emphasize that CDMFT fully incorporates the quantum many-body effects within a cluster (unit cell here). We thus cannot speak of sharp bands nor use topological indices based on Bloch states. Instead, we shall make use of the interacting Green’s function incorporating quantum fluctuations. We will corroborate the bulk-boundary correspondence for these correlated topological phases by examining the system in both infinite-size and slab geometries.

TURNING ON CORRELATIONS IN A TI

We first examine the bulk properties of the TI as U is turned on. The evolution of the phases together with their magnetization are shown in Fig. 1. The figure also shows a \mathbb{Z}_2 topological index Δ , which determines the presence ($\Delta = 1$) or absence ($\Delta = 0$) of a topological magneto-electric response. Specifically, $\Delta = 1$ implies that an applied electric field \mathbf{E} will induce a magnetization in a properly prepared system: $\mathbf{M} = \alpha \mathbf{E}$, where $\alpha = e^2/2h$ depends only on universal constants [14]. In the presence of TRS, this topological response can be used as a defining property of a correlated TI. The associated topological index can be computed from the full interacting Green’s function by the following Wess-Zumino-Witten like integral [14]

$$\Delta \stackrel{\text{mod } 2}{=} \frac{\pi}{3} \int_0^1 du \int \frac{d\omega}{2\pi} \int_{\text{BZ}} \frac{d^3\mathbf{k}}{(2\pi)^3} \text{Tr} \left[\epsilon^{\mu\nu\rho\sigma} \hat{G} \partial_\mu \hat{G}^{-1} \hat{G} \partial_\nu \hat{G}^{-1} \hat{G} \partial_\rho \hat{G}^{-1} \hat{G} \partial_\sigma \hat{G}^{-1} \hat{G} \partial_u \hat{G}^{-1} \right]. \quad (2)$$

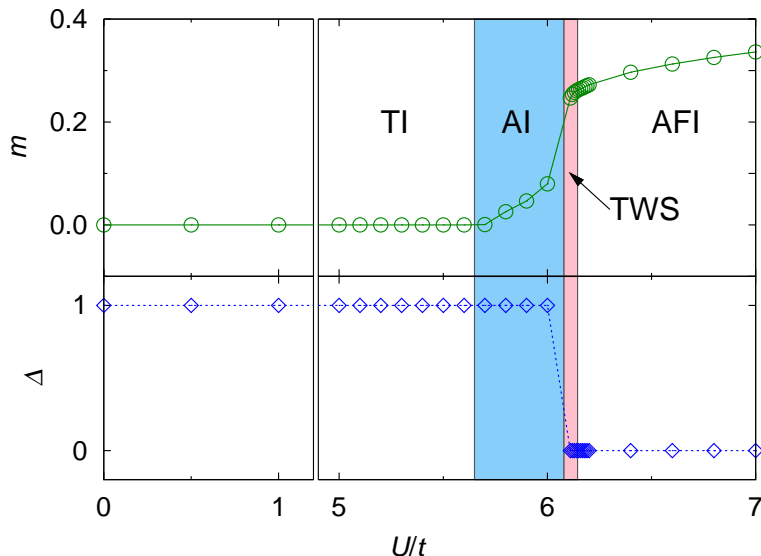


FIG. 1. **Magnetization (m) and topological index (Δ) versus interaction strength.** An interaction-driven topological transition accompanies an abrupt change of the magnetization. The nontrivial electronic structure of a correlated TI can be characterized by a \mathbb{Z}_2 -invariant computed using the CDMFT Green's function. In the intermediate region, a topologically nontrivial insulator with a finite magnetization indicates the realization of an interacting axion insulator (AI). As the interaction strength increases, a topological Weyl semimetal (TWS) follows after the magnetization jump. At large U , the system is a topologically-trivial insulating antiferromagnet (AF). (Note: the region $1 < U/t < 5$ has been truncated to emphasize the phases around the transition.)

The hat on the Green's function, \hat{G} , denotes the 8 by 8 matrix structure due to the pseudospin (σ) and sublattice ($1 \leq i \leq 4$) degrees of freedom. The parameter u extends the true Green's function at $u = 0$ to a trivial constant one at $u = 1$. It has been shown recently that in the special case where inversion symmetry is present, as is the case in this work, one can significantly simplify the above expression [18]:

$$(-1)^\Delta = \prod_{\mathbf{R}=\text{zero}} \eta_\alpha^{1/2}, \quad (3)$$

where $\eta_\alpha = \pm 1$ is a parity eigenvalue corresponding to a vector $|\alpha\rangle$, an *eigenstate of the interacting Green's function* evaluated at one of eight special momenta, $\mathbf{\Gamma}_i$. These are the time reversal invariant momenta (TRIM) satisfying $-\mathbf{\Gamma}_i = \mathbf{\Gamma}_i$, up to a reciprocal lattice vector. The expression Eq. (3) is in contrast with the analogous Fu-Kane formula which can only be used for non-interacting systems. More details about Δ , such as the notion of “R-zero”, can be found in the Supplementary Material.

From Fig. 1 we can see that the invariant indicates a topologically non-trivial phase for a wide range of onsite repulsion until a trivial phase results in the magnetic antiferromagnet, found at large U . It can be noted that the topological index remains invariant under the evolution of the Green's function due to interactions, such as spectral broadening. Eventually, a time-reversal-symmetry (TRS) breaking transition occurs, and there is a quantum phase transition out of the TI. From Fig. 1, we note that there is a regime where the magnetization increases continuously from zero before jumping discontinuously at $U/t = 6.11$. The latter jump, where the order parameter has a sudden increase even though TRS has already been broken, signals a first order transition. We have verified that it is a robust property within our framework. Figure 1 also shows that there is a small range of U where $\Delta = 1$, yet the system is magnetized. Because of the breaking of TRS, one cannot call this a topological insulator in the above sense. Rather this is a closely-related phase: a *correlated axion insulator*. It was introduced at the non-interacting level by Refs. [6, 19], where it was noted that even in the absence of TRS, by virtue of inversion symmetry and a special structure of the parity eigenvalues, the topological magneto-electric effect discussed above could be realized. Contrary to the TI, this phase does not have protected boundary states. As discussed in the Supplementary Material, the Δ -invariant, Eq. (3), is a natural generalization of the one introduced in Refs. [19, 20] as it essentially counts the total number of odd-parity eigenstates, not only one per Kramers pair. We add that one expects such a phase to be present if the magnetization increases continuously from a TI, because the parity structure is not expected to change dramatically. Finally, as the continuous transition preceding the first order one is a feature that is absent from the

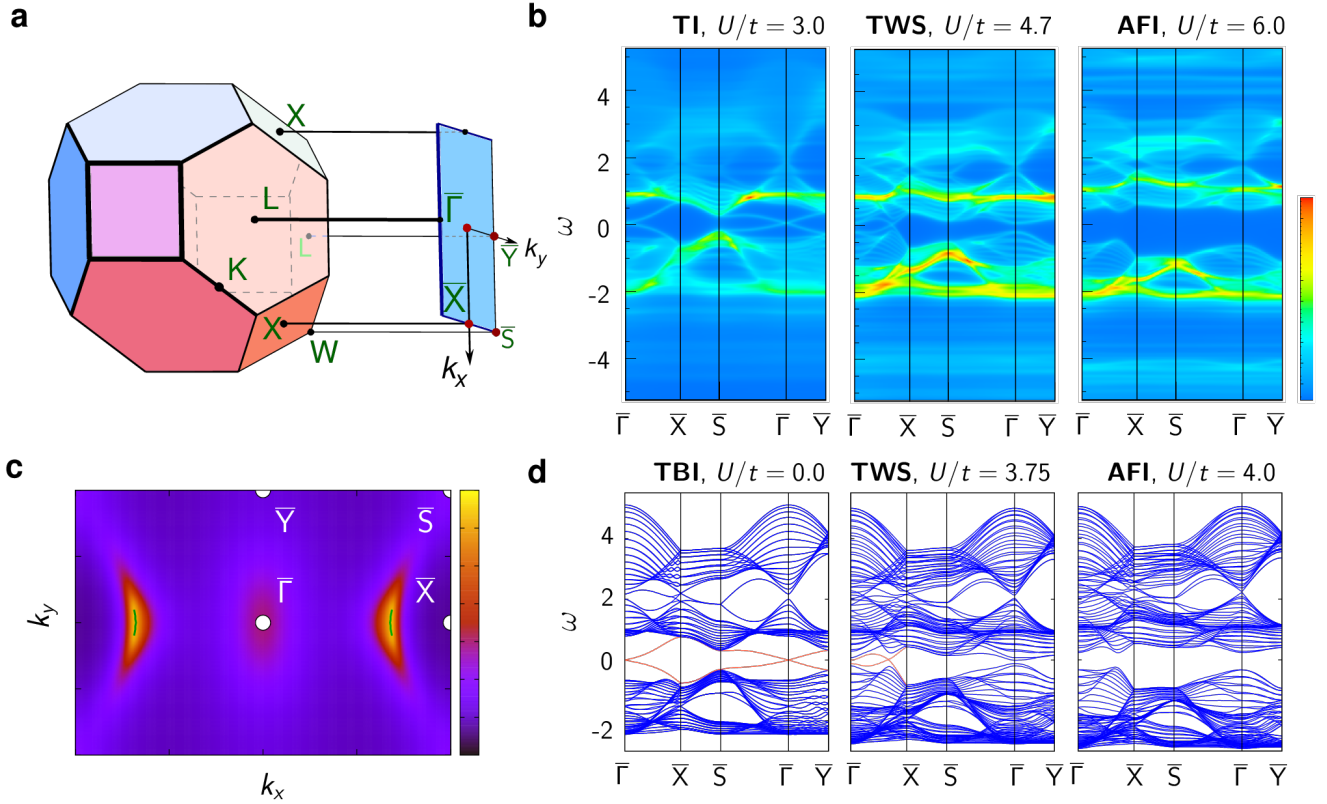


FIG. 2. **Surface states of a slab normal to (110).** **a**, First Brillouin zone (BZ) of a pyrochlore lattice and its projection onto the (110)-surface BZ. High symmetry points are labeled. **b**, Density plot of the surface spectral functions along lines connecting high-symmetry points. From left to right, the panels represent a topological insulator (TI), a topological Weyl semimetal (TWS), and an antiferromagnetic insulator (AFI). The spectral weight for each panel is renormalized by its maximal value for clarity. **c**, Spectral weight at the Fermi level, $\omega = 0$, for the TWS with $U/t = 4.7$. Fermi arcs crossing $k_y = 0$ clearly appear. The position of the arcs is roughly consistent with the HF result, denoted by green lines. **d**, Dispersion of the slab within the HF approximation. The red lines denote the surface states. The panels are in correspondence with those in **b**.

HF mean-field theory, this axion phase is fundamentally correlation driven.

TI surface states

Another route to examining the non-trivial topology of the ground state is via the bulk-boundary correspondence which, at the non-interacting level, guarantees the existence of protected surface states on any boundary with a trivial insulator, such as the vacuum. We verify this correspondence at the interacting level by performing a real space CDMFT calculation [17] on a slab that is finite along one direction. We solve for the layer-dependent Green's function self-consistently. For the details regarding the implementation of the slab calculation, please see the Supplementary Material. Due to the finiteness of the system in one direction, the transitions occur at slightly different values of U when compared with the bulk analysis, which prevents an exact one-to-one comparison. Notwithstanding, we proceed to argue that a clear correspondence exists between the two.

Figure 2 shows that the surface states persist as correlations are increased. The spectral function clearly displays sharp states crossing the bulk gap. Eventually the slab system undergoes a first order transition to a TWS. Note that the axion insulating phase presented in the above discussion for the bulk Hamiltonian is absent for the slab as there is no continuous rise of the magnetization. We attribute this to the finiteness of the system in one direction and expect the continuous transition to be recovered as one introduces more layers. We discuss the correlated TWS in the following section.

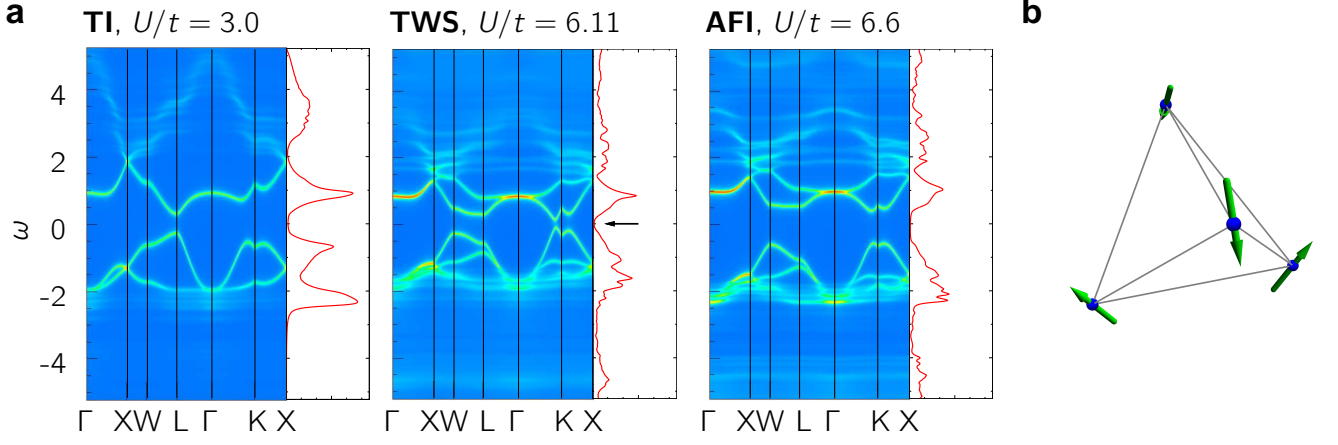


FIG. 3. **Bulk spectral function, local density of states and magnetic order for $t_\sigma = 1$.** **a**, Spectral weights along high symmetry lines and local density of states for three different values of interaction strength. The panels represent a TI, a TWS, and an insulating AF. These last two phases break TRS. In the TWS, the Weyl points are not along high symmetry lines, however, the density of states shows a quadratic scaling indicating their presence, as shown by the arrow. **b**, Magnetic ordering present for $U/t \geq 5.6$.

CORRELATED TOPOLOGICAL WEYL SEMIMETAL

After the magnetization jump in Fig. 1, the spectral gap closes and one obtains a region of TWS before the insulating AF at large U . We will analyze the fate of the TWS as we include correlations, which are expected to have a larger role than in the TI as the TWS is gapless.

The topological Weyl semimetal, as introduced at the non-interacting level [6], is a gapless state with a Fermi surface consisting of points (called Weyl points) around which the dispersion is linear. It can thus be viewed as a 3D analogue to graphene. Contrary to the Dirac points of graphene, the Weyl points are topologically robust as no local perturbation can gap them, as long as two Weyl points of opposite chirality do not merge. At the non-interaction level, given a Bloch Hamiltonian for an isotropic Weyl point at $\mathbf{k} = 0$, $H = \pm \mathbf{k} \cdot \boldsymbol{\tau}$, the chirality is ± 1 . $\boldsymbol{\tau}$ is a three-vector of Pauli matrices acting on the space of the two bands touching at $E = 0$. (The definition of chirality is analogous for a non-isotropic Weyl touching.) The protection of the Weyl node comes from the fact that only two bands meet at a point in three dimensions: all Pauli matrices have been used and an additional perturbation can only move the touching in the BZ. A fingerprint of the singular dispersion of the TWS is that it harbors chiral surface states which take the form of Fermi arcs in the surface BZ [6], reminiscent of those found in the pseudo-gap phase of the cuprates.

At the level of the bulk calculation, we have determined that the spectral gap closes and the density of states shows a quadratic vanishing at the Fermi level Fig. 3a, as is expected from linearly dispersing fermions in 3D. The eight Weyl points are not along high symmetry directions, hence Fig. 3a does not show the states of interest.

A decisive signature of the correlated Weyl phase comes from the surface state calculation. We again consider a slab with surfaces normal to the (110) direction. We find clear Fermi arcs arising from states localized on the surfaces, Fig. 2a. The arcs are broadened compared to the sharp lines found at the non-interacting level, see Fig. 2b. From the non-interacting theory we know that the arcs should join the projected bulk Weyl points on the surface BZ. Moreover, if for a given surface two Weyl points of opposite chiral charge are projected onto each other, no Fermi arc should arise from that point. In Fig. 2a, only two arcs can be seen for two reasons: first, the arcs coming from the top and bottom surfaces overlap too much to be distinguished; second, two pairs of opposite chirality are annihilated upon projection. We thus establish that the rule for the projection holds in the correlated phase, i.e. the notion of chirality for the quasiparticles persists.

WEYL TILTING AND MOTT TRANSITION

We briefly discuss the other phases in our Hubbard Hamiltonian corresponding to the second set of hopping parameters. When the non-interacting system is in a (semi)metallic state, HF calculations have shown that a second order transition occurs to an all-in/all-out magnetic order as U is included. As the effects of the onsite repulsion are

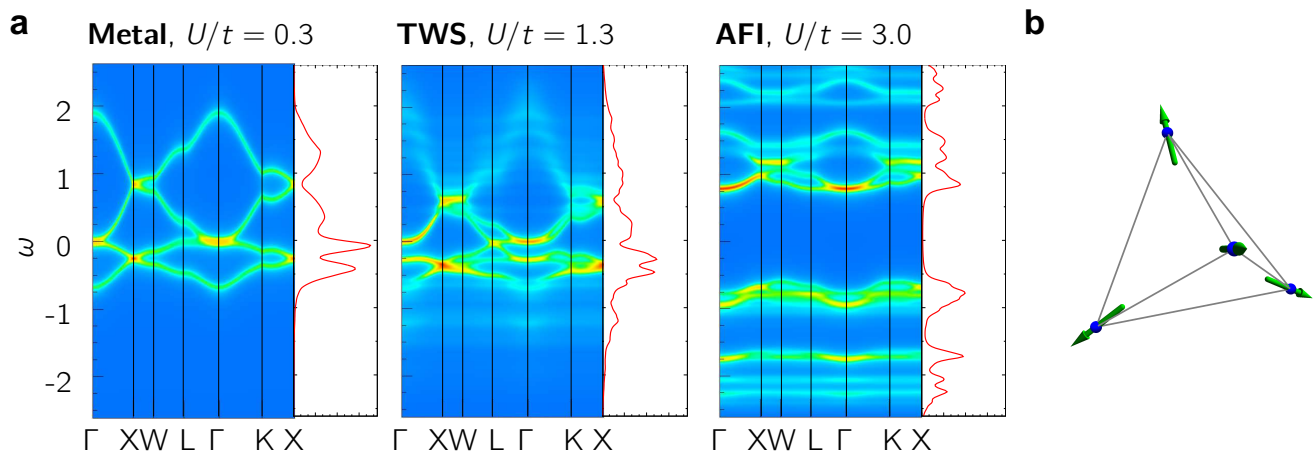


FIG. 4. **Bulk spectral function, local density of states and magnetic order for $t_\sigma = -1$.** **a**, The onsite repulsion drives the non-interacting metal into a “tilted Weyl semimetal”, as shown in the middle panel. The semimetallic behavior is destroyed at large U/t and the system becomes an antiferromagnetic insulator (AFI). **b**, The all-in/all-out magnetic ordering is stabilized with strong enough interaction.

expected to be stronger on a gapless phase, we perform a CDMFT calculation to examine its precise consequences. The resulting spectral function and local density of states are displayed in Fig. 4a. We find that the transition to the AF is second order. The same all-in/all-out configuration is found, as shown in Fig. 4b. Before the AF Mott insulator, a small region of “tilted Weyl semimetal” is found. By “tilted”, we mean that the dispersion of the Weyl quasiparticles is flat along certain directions. This effect was identified in the HF calculation and it was shown that second nearest hopping can remove the flatness [13]. A salient feature is that the effect of the local Coulomb repulsion is stronger in the semimetal as compared with the TI. Indeed we observe spectral broadening near the Fermi level at modest values of U , as can be seen in Fig. 4a.

DISCUSSION

We have so far mainly focused on theoretical studies of correlation effects on topological phases such as topological insulators and Weyl semimetals. Indeed, we have established the robustness of TIs from both sides of the bulk-boundary duality. A bulk topological invariant defined in terms of interacting Green’s functions was explicitly evaluated. We determined its change at a correlation driven topological transition to a trivial AF insulator. This invariant was used to predict the existence of a correlated axion phase at the onset of a continuous magnetic transition. From the boundary perspective, our work has shown that the surface states of both TIs and topological Weyl semimetals remain robust to interactions.

We now turn to the experimental considerations. The model we used is applicable to a large class of complex oxides, the pyrochlore iridates. These show metal-insulator transitions as the rare earth is changed [21] or pressure [22] applied. There are indications that some members of the family magnetically order at low temperatures [23–27]. However, it is still not clear what the nature of the ordering is, if any. Diverse ground states can be realized as a result of the effects of chemical and physical pressure on the electronic structure. As correlations can play an important role in the determination of these ground states, it is important to understand their precise effect. Our work goes beyond the non-interacting and mean-field studies done previously and establishes not only the presence but also the stability of various topological phases with the inclusion of strong correlations. Moreover, we predict that the axion insulator might be realized due to the presence of a correlation-driven second order transition preceding a first order one. In this phase, the surface states are gapped and the quantized magneto-electric effect exists even though the bulk is magnetically ordered. In future work, we shall consider further signatures of correlations in these phases by studying the optical conductivity, for instance.

The methods used in this paper, CDMFT (bulk and real space) and topological response computed using Green’s functions, can be used for a wide class of complex oxides, not only those mentioned above. We suggest that these tools can be applied to examine generic interacting states with symmetry-protected topological order and combined

with *ab initio* tools in the quest for experimentally relevant candidate materials.

ACKNOWLEDGEMENTS

This work was supported by the National Research Foundation of Korea (NRF) funded by the Korea government (MEST) through the Quantum Metamaterials Research Center, No. 2011-0000982 and Basic Science Research, No. 2010-0010937 (AG, GSJ), NSERC, the Canada Research Chair program, and the Canadian Institute for Advanced Research (WWK,YBK), FQRNT and the Walter Sumner Foundation (WWK), NRF, No. 2008-0062238 (KP). The numerical computations were done in Seoul National University and SciNet at the University of Toronto.

SUPPLEMENTARY MATERIAL

Cellular dynamical mean-field theory

Cellular dynamical mean-field theory (CDMFT) reduces infinite lattice to a cluster of size N_c which hybridizes with the self-consistent electronic bath sites. It extends single-site DMFT with the goal of capturing spatial correlations more adequately. In this work, we used a tetrahedron cluster with 4 sites, which corresponds to a unit cell of the pyrochlore lattice. Figure 5 illustrates the cluster which is embedded in an effective, self-consistent bath. In order to investigate the ground state properties, we employ the exact diagonalization method to fully solve the quantum many-body properties of the cluster. The algorithm is iterative in nature: we initially input an ansatz for the bath parameters and solve the hybridized Hamiltonian with the impurity solver. From the cluster Hamiltonian we compute the cluster Green function \hat{G} , the hat denoting an 8×8 matrix structure, as well as the cluster self-energy, $\hat{\Sigma}^c = \hat{G}^{-1} - \hat{G}^{-1}$, where \hat{G} is the Weiss field describing the noninteracting bath. The new Weiss field is obtained by the self-consistent equation, $\hat{G}_{\text{new}}^{-1} = \hat{G}_{\text{loc}}^{-1} + \hat{\Sigma}^c$, where the local Green function

$$\hat{G}_{\text{loc}}(i\omega_n) = \sum_{\mathbf{k}} \left[(i\omega_n + \mu) \hat{1} - \hat{t}(\mathbf{k}) - \hat{\Sigma}^c(i\omega_n) \right]^{-1} \quad (4)$$

is calculated by integration over the momentum vector of the reduced Brillouin zone. We then determine new bath parameters to best fit \hat{G}_{new} . The steps are repeated until convergence is reached.

The calculation for a slab structure is similar to the bulk case, but the Green's function is now an $8L \times 8L$ matrix.

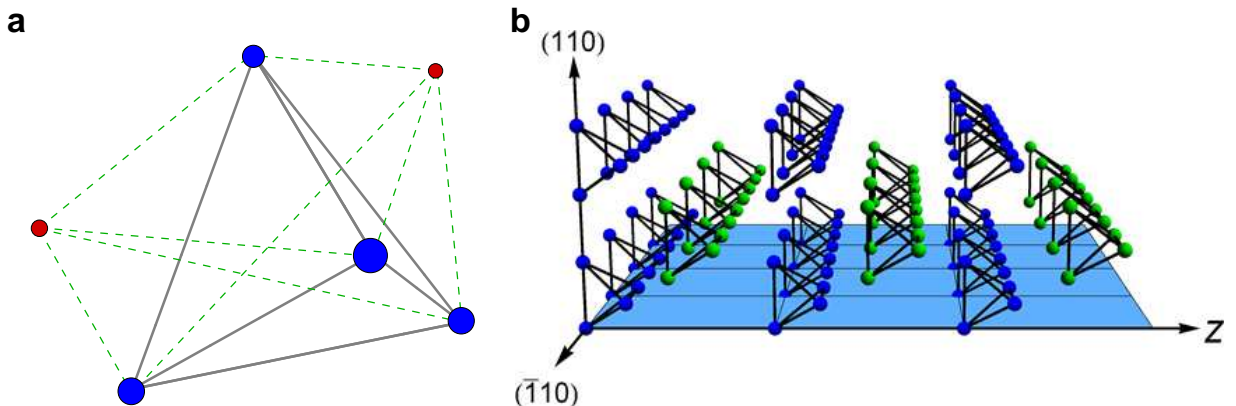


FIG. 5. **CDMFT cluster and slab geometry.** **a**, Unit tetrahedron (cluster) and bath sites. Only $N_b = 2$ bath sites are shown while $N_b = 8$ (4) were used for the bulk and slab calculations, respectively. The blue and red spheres denote the cluster and the bath sites, respectively. The dashed green lines indicate the effective hybridization between the cluster and the bath. **b**, Three layers within a slab that is finite along the (110)-direction. The tetrahedra in each layer are colored alternately with blue or green. We use 16 layers with periodic boundary conditions for the other two directions which span the sky-blue plane.

The self-consistent equation for a slab with L layers is given by

$$\mathcal{G}_{0,\text{new}}^{-1}(i\omega_n) = \left[\sum_{k_x, k_y} \frac{1}{(i\omega_n + \mu)\mathbf{1} - \mathbf{t}(k_x, k_y) - \mathbf{\Sigma}(i\omega_n)} \right]^{-1} + \mathbf{\Sigma}(i\omega_n) \quad (5)$$

where bold letters denote an $8L \times 8L$ matrix structure and the summation runs over the surface Brillouin zone. We assume that the self-energy is block-diagonal with the blocks of size eight. The correlations beyond a unit cell are treated on the mean-field level. In other words, the sectors make an effect on each other via the hopping matrix \mathbf{t} , although each sector of the self-energy is self-consistently determined by its own cluster Hamiltonian,

$$\begin{aligned} H_c^p = & \sum_{\mu\nu\sigma} E_{\mu\nu}^p c_{p,\mu\sigma}^\dagger c_{p,\nu\sigma} + U \sum_{\mu} n_{p,\mu\uparrow} n_{p,\mu\downarrow} \\ & + \sum_{\mu l\sigma} (V_{p,\mu l\sigma}^p a_{p,l\sigma}^\dagger c_{p,\mu\sigma} + H.c.) + \sum_{l\sigma} \epsilon_{l\sigma}^p a_{p,l\sigma}^\dagger a_{p,l\sigma}, \end{aligned} \quad (6)$$

where $\mu, \nu = 1, 2, \dots, 4$ are the site indices in a unit cell, $l = 1, 2, \dots, N_b$ label the bath sites, and $p = 1, \dots, L$ is a layer index. The hoppings within a cluster and chemical potential are introduced by \hat{E} while the L -effective Weiss fields are described by the V 's and ϵ 's.

Topological invariant Δ

We provide information on the implementation of the topological invariant Δ [18] and its usage in the absence of TRS. For clarity, we rewrite it here,

$$(-1)^\Delta = \prod_{\text{R-zero}} \eta_\alpha^{1/2} \quad (7)$$

As was noted in the main text, $\eta_\alpha = \pm 1$ is a parity eigenvalue corresponding to an eigenstate, $|\alpha\rangle$, of the inverse of the interacting Green's function, \hat{G}^{-1} , evaluated at one of eight TRIM, $\mathbf{\Gamma}_i$. We now explain the notion of ‘‘Right-zero’’ (R-zero). The eigenvector satisfies:

$$\hat{G}^{-1}(\omega, \mathbf{\Gamma}_i) |\alpha(\omega, \mathbf{\Gamma}_i)\rangle = \mu_\alpha(\omega, \mathbf{\Gamma}_i) |\alpha(\omega, \mathbf{\Gamma}_i)\rangle \quad (8)$$

$$\hat{P} |\alpha(\omega, \mathbf{\Gamma}_i)\rangle = \eta_\alpha |\alpha(\omega, \mathbf{\Gamma}_i)\rangle \quad (9)$$

where $\hat{G}^{-1}(\omega, \mathbf{k})$ is the inverse Green's function, $\mu_\alpha(\omega, \mathbf{k})$ is its generally complex eigenvalue, and \hat{P} the parity operator. As ω is tuned from $-\infty$ to ∞ , $\mu_\alpha(\omega, \mathbf{k})$ sweeps a curve. At $\omega = 0$, $\hat{G}^{-1}(0, \mathbf{k})$ is Hermitian hence its eigenvalues are real. $\mu_\alpha(0, \mathbf{k})$ thus crosses the real axis in the complex plane and in this sense is called a ‘‘zero’’. It is a R-zero simply if the crossing occurs to the right of the imaginary axis, i.e.

$$\text{R-zero} \Leftrightarrow \mu_\alpha(0, \mathbf{k}) > 0 \quad (10)$$

Hence, if $\mu_\alpha(0, \mathbf{\Gamma}_i)$ is a R-zero, the associated parity eigenvalue η_α will contribute to the product for $(-1)^\Delta$ above.

In the presence of TRS, each $|\alpha(0, \mathbf{\Gamma}_i)\rangle$ has a time-reversal partner with the same eigenvalue μ_α [18]. Hence, each of the Kramers pairs of odd-parity eigenstates contributes $i^2 = -1$, and the index can only be zero or one. When one breaks TRS, the R-zeroes need not come in Kramers pairs. However, we argue that even in that case, as long as inversion symmetry is preserved, the topological index can still be used to test for the presence of a quantized magneto-electric response. An insulator with TRS broken but with such a response is called an axion insulator [6, 19]. The applicability of Δ for such inversion-symmetric topological insulators was briefly suggested in Ref. [18].

When TRS is broken, one needs to first ensure that Δ remains 0 or 1, avoiding imaginary values for instance. The equivalent statement for band insulators was established by Refs. [19, 20] who proved that inversion symmetric band insulators always have an even number of odd-parity occupied states (including all TRIM). For correlated inversion-symmetric insulators, this would translate to the requirement to have an even number of odd-parity R-zeroes. This statement seems natural for insulators that are adiabatically connected to a band-insulator. With this constraint, we

TABLE I. Number of odd-parity *R-zeroes* per TRIM. The non-trivial Green's function topology characterizes the topological insulator (TI) and axion insulator (AI) phases. A topological transition occurs as the system enters the gapless TWS. The change happens at the four *L* points.

<i>U</i>	Phase	Γ	X, Y, Z	L'	$L(\times 3)$	N_o
0.00	TI	0	2	4	0	10
3.00	TI	0	2	4	0	10
6.00	AI	0	2	4	0	10
6.11	TWS	0	2	3	1	12
8.00	AFI	0	2	3	1	12

can write an equivalent expression for Δ :

$$\Delta = \frac{N_o}{2} \mod 2 \quad (11)$$

where N_o is the total (even) number of odd-parity R-zeroes at the TRIM. This formula also applies to the TRS case. In other words, for an insulator, a necessary condition to have a topologically non-trivial magneto-electric response is that N_o be twice an odd number. In the presence of TRS it is sufficient and we have the TI discussed above. Otherwise, one also needs to ascertain that the Hall conductivities vanish.

We describe the evolution of the parities, and hence of Δ , as we increase U in the TI, see Table I. At $U = 0$, we have a topological band insulator and Eq. (7) reduces to the Fu-Kane index, ν_0 [28]. Indeed, the condition of being a R-zero then implies an occupied Bloch state at the given TRIM. For $U > 0$, we use the interacting Green's function to compute Δ and find that its parity structure does not change as long as the state remains insulating. This must be so as the gap does not close, hence none of the eigenvalues of $\hat{G}^{-1}(0, \mathbf{\Gamma}_i)$ can vanish. Eventually, TRS is spontaneously broken but continuously. For small values of the magnetization, not surprisingly, the parity structure is not affected and we thus have an axion insulator. The magnetization jumps at the first order transition. The large magnetization after the transition alters number of odd-parity R-zeroes at the *L* points such that $\Delta = 0$ because $N_o = 2 \times 6$. Strictly speaking, one should not evaluate Δ near the transition as the system is gapless there, being in a TWS phase. Eventually, a gap opens leaving behind a trivial antiferromagnetic insulator (AFI).

-
- [1] M. Z. Hasan and C. L. Kane, Rev. Mod. Phys. **82**, 3045 (2010).
 - [2] X.-L. Qi and S.-C. Zhang, Rev. Mod. Phys. **83**, 1057 (2011).
 - [3] A. M. Turner, Y. Zhang, and A. Vishwanath, Phys. Rev. B **82**, 241102 (2010).
 - [4] G. Kotliar, S. Y. Savrasov, G. Pálsson, and G. Biroli, Phys. Rev. Lett. **87**, 186401 (2001).
 - [5] T. Maier, M. Jarrell, T. Pruschke, and M. H. Hettler, Rev. Mod. Phys. **77**, 1027 (2005).
 - [6] X. Wan, A. M. Turner, A. Vishwanath, and S. Y. Savrasov, Phys. Rev. B **83**, 205101 (2011).
 - [7] L. Balents, Physics **4**, 36 (2011).
 - [8] A. A. Burkov and L. Balents, Phys. Rev. Lett. **107**, 127205 (2011).
 - [9] K.-Y. Yang, Y.-M. Lu, and Y. Ran, Phys. Rev. B **84**, 075129 (2011).
 - [10] D. Pesin and L. Balents, Nature Phys. **6**, 376 (2010).
 - [11] B.-J. Yang and Y. B. Kim, Phys. Rev. B **82**, 085111 (2010).
 - [12] M. Kargarian, J. Wen, and G. A. Fiete, Phys. Rev. B **83**, 165112 (2011).
 - [13] W. Witczak-Krempa and Y. B. Kim, Phys. Rev. B **85**, 045124 (2012).
 - [14] X.-L. Qi, T. L. Hughes, and S.-C. Zhang, Phys. Rev. B **78**, 195424 (2008).
 - [15] G. Kotliar, S. Y. Savrasov, K. Haule, V. S. Oudovenko, O. Parcollet, and C. A. Marianetti, Rev. Mod. Phys. **78**, 865 (2006).
 - [16] B. J. Kim, H. Ohsumi, T. Komesu, S. Sakai, T. Morita, H. Takagi, and T. Arima, Science **323**, 1329 (2009).
 - [17] W. Wu, S. Rachel, W.-M. Liu, and K. Le Hur, "Quantum spin Hall insulators with interactions and lattice anisotropy," (2011), arXiv:1106.0943.
 - [18] Z. Wang, X.-L. Qi, and S.-C. Zhang, (2012), arXiv:1201.6431v2.
 - [19] A. M. Turner, Z. Yi, R. S. K. Mong, and A. Vishwanath, (2010), arXiv:1010.4335v2.
 - [20] T. L. Hughes, E. Prodan, and B. A. Bernevig, Phys. Rev. B **83**, 245132 (2011).
 - [21] D. Yanagishima and Y. Maeno, J. Phys. Soc. Jpn. **70**, 2880 (2001).

- [22] F. F. Tafti, J. J. Ishikawa, A. McCollam, S. Nakatsuji, and S. R. Julian, (2011), arXiv:1107.2544.
- [23] S. Zhao, J. M. Mackie, D. E. MacLaughlin, O. O. Bernal, J. J. Ishikawa, Y. Ohta, and S. Nakatsuji, Phys. Rev. B **83**, 180402 (2011).
- [24] K. Tomiyasu, K. Matsuhira, K. Iwasa, M. Watahiki, S. Takagi, M. Wakeshima, Y. Hinatsu, M. Yokoyama, K. Ohoyama, and K. Yamada, (2011), arXiv:1110.6605.
- [25] M. C. Shapiro, S. C. Riggs, M. B. Stone, C. R. d. l. Cruz, S. Chi, A. A. Podlesnyak, and I. R. Fisher, (2012), arXiv:1201.5419.
- [26] S. M. Disseler, C. Dhital, T. C. Hogan, A. Amato, S. R. Giblin, C. d. Cruz, A. Daoud-Aladine, S. D. Wilson, and M. J. Graf, (2012), arXiv:1201.4606.
- [27] T. F. Qi, O. B. Korneta, X. Wan, and G. Cao, (2012), arXiv:1201.0538.
- [28] L. Fu and C. L. Kane, Phys. Rev. B **76**, 045302 (2007).

